Dalton Transactions

Accepted Manuscript

This article can be cited before page numbers have been issued, to do this please use: B. Warajtis, B. . Gliši, N. D. Savi, A. Pavic, S. Vojnovic, A. M. Veselinovi, J. Nikodinovic-Runic, U. Rychlewska and M. I. Djuran, *Dalton Trans.*, 2017, DOI: 10.1039/C6DT04862E.

This is an Accepted Manuscript, which has been through the Royal Society of Chemistry peer review process and has been accepted for publication.

Accepted Manuscripts are published online shortly after acceptance, before technical editing, formatting and proof reading. Using this free service, authors can make their results available to the community, in citable form, before we publish the edited article. We will replace this Accepted Manuscript with the edited and formatted Advance Article as soon as it is available.

You can find more information about Accepted Manuscripts in the author guidelines.

Please note that technical editing may introduce minor changes to the text and/or graphics, which may alter content. The journal's standard Terms & Conditions and the ethical guidelines, outlined in our author and reviewer resource centre, still apply. In no event shall the Royal Society of Chemistry be held responsible for any errors or omissions in this Accepted Manuscript or any consequences arising from the use of any information it contains.

ROYAL SOCIETY OF CHEMISTRY

rsc.li/dalton

View Article Online
DOI: 10.1039/C6DT04862E

Journal Name

ARTICLE

Mononuclear gold(III) complexes with L-histidine-containing dipeptides: tuning the structural and biological properties by variation of the N-terminal amino acid and counter anion†

Received 00th January 20xx,
Accepted 00th January 20xx

DOI: 10.1039/x0xx00000x

www.rsc.org/

Beata Warżajtis,[a] Biljana Đ. Glišić,[b] Nada D. Savić,[b] Aleksandar Pavić,[c] Sandra Vojnovic,[c] Aleksandar Veselinović,[d] Jasmina Nikodinovic-Runic,*[c] Urszula Rychlewska*[a] and Miloš I. Djuran*[b]

Gold(III) complexes with different L-histidine-containing dipeptides, [Au(Gly-L-His-N_A,N_P,*N3*)Cl]Cl·3H_2O (**1a**), [Au(Gly-L-His-N_A,N_P,*N3*)Cl]NO_3·1.25H_2O (**1b**), [Au(L-Ala-L-His-N_A,N_P,*N3*)Cl][$AuCl_4$]·H_2O (**2a**), [Au(L-Ala-L-His-N_A,N_P,*N3*)Cl]NO_3·2.5H_2O (**2b**), [Au(L-Val-L-His-N_A,N_P,*N3*)Cl]Cl·2H_2O (**3**), [Au(L-Leu-L-His-N_A,N_P,*N3*)Cl]Cl (**4a**) and [Au(L-Leu-L-His-N_A,N_P,*N3*)Cl][$AuCl_4$]·H_2O (**4b**) have been synthesized and structurally characterized by spectroscopic (^{1}H NMR, IR and UV-vis) and single-crystal X-ray diffraction techniques. The antimicrobial efficiency of these gold(III) complexes, along with K[$AuCl_4$] and the corresponding dipeptides, was evaluated against the broad panel of Gram-positive and Gram-negative bacteria and fungi, displaying their moderate inhibiting activity. Moreover, cytotoxic properties of the investigated complexes were assessed against the normal human lung fibroblast cell line (MRC5) and two human cancer, cervix (HeLa) and lung (A549) cell lines. None of the complexes exerted significant cytotoxic activity; nevertheless complexes that did show selectivity in terms of cancer *vs.* normal cell lines (**2a**/**b** and **4a**/**b**) have been evaluated using zebrafish (*Danio rerio*) embryos for toxicity and antiangiogenic potential. Although the gold(III) complexes achieved antiangiogenic effect comparable to the known angiogenic inhibitors auranofin and sunitinib malate at 30-fold higher concentrations, they had no cardiovascular side effects, which commonly accompany auranofin and sunitinib malate treatment. Finally, binding of the gold(III) complexes to the active sites of both human and bacterial (*Escherichia coli*) thioredoxin reductases (TrxRs) was demonstrated by molecular docking study, suggesting that the mechanism of biological action of these complexes can be associated with their interaction with the TrxR active site.

Introduction

Among the twenty proteinogenic amino acids, L-histidine (L-His) plays a crucial role in biological systems due to its aromatic imidazole moiety, which is a common coordinating ligand in metalloproteins and a part of the catalytic site in several enzymes.[1-3] The heterocyclic imidazole system in the L-histidine provides two competitive nitrogen donor atoms, designated as N1 and N3. Thus, in some metalloproteins, metal ion is bound to the imidazole ring through N1 nitrogen only (Fe(II) in hemoglobin),[4] while in the active site of the others, imidazole ring is coordinated through N3 (Zn(II) in superoxide dismutase).[5] Besides that, a metal ion can have a mixed donor site sphere, as Cu(II) in superoxide dismutase ($(N3)_2$, $N1_{term}$, $N1_{bridge}$),[5] or in some metalloproteins the same metal ion displays different environments ($Cu_1(N3)_2$ and $Cu_3(N1)_8$ in ascorbate oxidase).[6] In majority of metal complexes with L-histidine-containing ligands, such as copper(II),[7] platinum(II)[8] and palladium(II)[9-11] complexes with glycyl-L-histidine (Gly-L-His), the imidazole ring is coordinated to the corresponding metal ion through the N3 nitrogen. Complexes, in which histidine is coordinated through the N1 nitrogen, are relatively rare.[12-18]

Peptides containing L-histidine amino acid have been shown as good chelating ligands for Au(III) ion.[9,19-22] Although reactions of the Au(III) ion with these peptides have been extensively investigated,[19-22] only a few gold(III)–peptide complexes were synthesized and characterized by single-crystal X-ray diffraction analysis.[9,19,20] Crystallographic results for gold(III) complexes with L-histidine-containing peptides showed that these peptides are coordinated to the Au(III) ion through the N3 imidazole nitrogen, the deprotonated nitrogen of the amide bond(s) (N_P) and to the nitrogen of the N-terminal amino group (N_A). From the previous studies,[9,19,20] it

[a] Faculty of Chemistry, Adam Mickiewicz University, Umultowska 89B, 61-614 Poznań, Poland; E-mail: urszular@amu.edu.pl
[b] Department of Chemistry, Faculty of Science, University of Kragujevac, R. Domanovića 12, 34000 Kragujevac, Serbia; E-mail: djuran@kg.ac.rs
[c] Institute of Molecular Genetics and Genetic Engineering, University of Belgrade, Vojvode Stepe 444a, 11000 Belgrade, Serbia; E-mail: jasmina.nikodinovic@gmail.com
[d] Faculty of Medicine, Department of Chemistry, University of Niš, 18000 Niš, Serbia
† Electronic Supplementary Information (ESI) available: Fig. S1-S5 and Table S1-S6. See DOI: 10.1039/x0xx00000x
CCDC 1523450-1523453 contains the supplementary crystallographic data for this paper. These data can be obtained free of charge from The Cambridge Crystallographic Data Centre via https://www.ccdc.cam.ac.uk/data_request/cif.

View Article Online
DOI: 10.1039/C6DT04862E

was confirmed that the N3-anchored Au(III) ion was able to deprotonate amide nitrogen in L-histidine-containing peptides even at pH < 2.00. Moreover, it was shown that these peptides were more reactive with Au(III) than those containing no heteroatom in the side chain.[23] Difference in the reactivity between these two types of peptides resulted from the fact that the N3-histidine anchoring the Au(III) ion was more effective at displacing the amide proton than Au(III) attached to either carboxylate oxygen or terminal amino nitrogen atom in no-histidine-containing peptides.[23] On the basis of spectroscopic measurements, it was found that coordination of L-histidine-containing peptides stabilizes Au(III) ion and prevents its reduction to the Au(I)/Au(0) under physiological conditions.[24]

Gold species have found their application in chrysotherapy, whereby complexes containing gold in the oxidation state +1 are applied to reduce inflammation and disease progress in patients with rheumatoid arthritis.[25,26] Clinically approved gold(I) complex, auranofin (2,3,4,6-tetra-*o*-acetyl-1-thio-β-D-glucopyranosato-S-(triethylphosphine)gold(I)), utilized in therapy of severe rheumatoid arthritis since 1985, has also shown anticancer potential[27] and was recently proven to be potent antimicrobial agent for the treatment of staphylococcal infections.[28] Furthermore, it was found that auranofin exerts broad-spectrum bactericidal activities by targeting thiol-redox homeostasis in species such as *Mycobacterium tuberculosis*, *Bacillus subtilis*, *Enterococcus faecium* and methicillin-resistant *Staphylococcus aureus*.[29] Recent study has also described auranofin as potent antiangiogenic compound.[30]

It has been postulated that under physiological conditions, gold(I) species are more stable than the gold(III) ones, which are readily reduced to Au(I) and/or Au(0) by naturally occurring thiols and thioethers and various proteins.[26,31,32] Methionine oxidation to its sulfoxide in the presence of Au(III) has been evidenced by X-ray diffraction analysis.[33] The fact that Au(III) can act as relatively strong oxidizing agent has been connected to its inhibiting activity of various proteins.[25] The importance of coordination chemistry of Au(III) ion with L-histidine-containing peptides, and the finding that some of these complexes have shown promising cytotoxic activity toward different human tumor cell lines,[24] prompted us to study a series of gold(III) complexes with X-L-His dipeptides (X = Gly, L-Ala, L-Val and L-Leu), [Au(Gly-L-His-N_A,N_P,*N3*)Cl]Cl·3H_2O (**1a**), [Au(Gly-L-His-N_A,N_P,*N3*)Cl]NO_3·1.25H_2O (**1b**), [Au(L-Ala-L-His-N_A,N_P,*N3*)Cl][$AuCl_4$]·H_2O (**2a**), [Au(L-Ala-L-His-N_A,N_P,*N3*)Cl]NO_3·2.5H_2O (**2b**), [Au(L-Val-L-His-N_A,N_P,*N3*)Cl]Cl·2H_2O (**3**), [Au(L-Leu-L-His-N_A,N_P,*N3*)Cl]Cl (**4a**) and [Au(L-Leu-L-His-N_A,N_P,*N3*)Cl][$AuCl_4$]·H_2O (**4b**). Part of this data, including the crystal structures of **1a**, **1b** and **2b,** has already been reported.[19,20] Nevertheless, all seven complexes have been evaluated for their antimicrobial and cytotoxic properties, while the ones that showed the best selectivity index have been evaluated using zebrafish (*Danio rerio*) embryos for toxicity and antiangiogenic potential and their activity has been compared to that of the corresponding dipeptides, K[$AuCl_4$] and auranofin. In addition, *in silico* study was conducted to evaluate the potential of these complexes to bind both human and *Escherichia coli* thioredoxin reductases (TrxRs).

Results and discussion

Synthesis and spectroscopic characterization of the gold(III) complexes with L-histidine-containing dipeptides

Synthesis. Seven gold(III) complexes with L-histidine-containing dipeptides, [Au(Gly-L-His-N_A,N_P,*N3*)Cl]Cl·3H_2O (**1a**), [Au(Gly-L-His-N_A,N_P,*N3*)Cl]NO_3·1.25H_2O (**1b**), [Au(L-Ala-L-His-N_A,N_P,*N3*)Cl][$AuCl_4$]·H_2O (**2a**), [Au(L-Ala-L-His-N_A,N_P,*N3*)Cl]NO_3·2.5H_2O (**2b**), [Au(L-Val-L-His-N_A,N_P,*N3*)Cl]Cl·2H_2O (**3**), [Au(L-Leu-L-His-N_A,N_P,*N3*)Cl]Cl (**4a**) and [Au(L-Leu-L-His-N_A,N_P,*N3*)Cl][$AuCl_4$]·H_2O (**4b**) were synthesized according to the procedure presented in Scheme 1. The corresponding X-L-His dipeptide (X = Gly, L-Ala, L-Val and L-Leu) was mixed with an equimolar amount of K[$AuCl_4$] in water at the pH range 1.50 – 2.00 and room temperature. We have found previously that the rate of the reaction between the corresponding dipeptide and Au(III) increased with increasing the pH of solution.[23] However, when this reaction was performed at pH > 3.00, a reduction of Au(III) to Au(I) and Au(0) occurred during time. pH of the reaction mixture was adjusted by addition of 1 M HCl for **1a, 2a** and **4a** or 1 M HNO_3 for **1b, 2b** and **4b**, while in the reaction of L-Val-L-His dipeptide with K[$AuCl_4$], complex **3** was formed in the presence of both acids. The stoichiometries of all gold(III) complexes were confirmed by elemental microanalysis, and their structures were elucidated by ^{1}H NMR, IR and UV-vis spectroscopy. Proton NMR spectroscopic data of these complexes were correlated with those reported previously for **1b** and **2b**.[20] The crystal structures of complexes **2a**, **3**, **4a** and **4b** were determined by single-crystal X-ray diffraction analysis.

^{1}H NMR characterization. Ambient temperature ^{1}H NMR spectra of gold(III) complexes **1-4** and the corresponding L-histidine-containing dipeptides have been measured in D_2O at pD 2.95. The ^{1}H chemical and $\Delta(^1H)_{coord}$ coordination shifts for **1a**, **2a**, **3** and **4a**, determined in respect to those for the free peptides, are listed in Table 1. The proton NMR data of the complexes **1b**, **2b** and **4b** are almost identical to those of the corresponding **1a**, **2a** and **4a**, considering the fact that they differ only in the counter anion (Scheme 1). Furthermore, these data for the complexes **1b** and **2b** are in accordance with those reported previously for the same complexes, which structures have been determined by single-crystal X-ray diffraction analysis.[20]

In the aromatic region, ^{1}H NMR spectra of the complexes **1a**, **2a**, **3** and **4a** consist of two resonances corresponding to the C2H and C5H protons of the imidazole ring, with the chemical shifts slightly differing from those of the uncoordinated X-L-His dipeptides (Table 1). Previous studies related to the reactions of metal ions with this type of peptides have shown that the chemical shifts of the C2H and C5H imidazole protons are very good indicating parameters for binding of the metal center to the N3 or N1 imidazole nitrogen

DOI: 10.1039/C6DT04862E

atom.[34] As can be seen from Table 1, the resonances for C2H and C5H imidazole protons of the complexes **1a**, **2a**, **3** and **4a** are upfield shifted with respect to those for the free dipeptides. The larger coordination shifts were observed for the C2H ($\Delta\delta$ = 0.06 – 0.08 ppm) with respect to the C5H proton ($\Delta\delta$ = 0.00 – 0.04 ppm); this indicates that the binding center for Au(III) is imidazole N3 nitrogen. Contrary to the observed upfield shifting of the aromatic imidazole protons in **1a**, **2a**, **3** and **4a**, the coordination of X-L-His dipeptides to the Au(III) ion resulted in the downfield shifting of the aliphatic protons. However, as it was found previously for the complexes **1b** and **2b**,[20] differences in the chemical shifts of the aliphatic protons for the gold(III) complexes and the corresponding X-L-His dipeptides are not significant and are caused by the coordination of the N3 imidazole-anchored Au(III) ion to the deprotonated peptide nitrogen N_P and to the nitrogen atom of the terminal amino group N_A. The most notable difference in the spectra of the complexes with respect to those of the free peptides is the magnetic non-equivalence of the HisβCH$_2$ protons (Table 1), as a consequence of the six-membered N3,N_P-ring formation (Scheme 1).

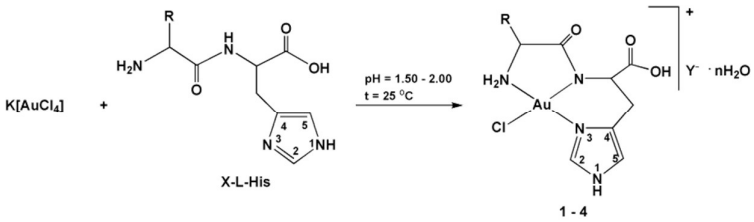

Au(III) complex	pH adjustment	X	R	Y$^-$	n
1a	HCl	Gly	H	Cl^-	3
1b	HNO_3	Gly	H	NO_3^-	1.25
2a	HCl	L-Ala	CH_3	$[AuCl_4]^-$	1
2b	HNO_3	L-Ala	CH_3	NO_3^-	2.5
3	HCl and HNO_3	L-Val	$CH(CH_3)_2$	Cl^-	2
4a	HCl	L-Leu	$CH_2CH(CH_3)_2$	Cl^-	0
4b	HNO_3	L-Leu	$CH_2CH(CH_3)_2$	$[AuCl_4]^-$	1

Scheme 1 Schematic presentation of the synthesis of gold(III) complexes with L-histidine-containing dipeptides. The numbering of atoms in the imidazole ring follows the IUPAC rules. n represents the number of crystalline water molecules.

Table 1 ^{1}H chemical and coordination shifts (in parentheses), alongside multiplicities and coupling constants ($J_{H\text{-}H}$), for X-L-His dipeptides (X = Gly, L-Ala, L-Val and L-Leu) and corresponding gold(III)-peptide complexes **1a, 2a, 3** and **4a** in D_2O as solvent with TSP as the internal standard measured at pD = 2.95. The NMR data of the complexes **1b, 2b** and **4b** are almost identical to those of the corresponding **1a**, **2a** and **4a**, respectively, and therefore not presented. *s* = singlet; *d* = doublet; *dd* = doublet of doublets; *t* = triplet; *q* = quartet; *m* =multiplet.

Peptide/Complex	Imidazole protons C2H (*s*)	C5H (*s*)	Chemical shifts of other protons				
			GlyCH_2			**HisαCH**	**HisβCH_2**
Gly-L-His	8.62	7.31	3.84, *s*			4.67, *t*, *J* = 5.6 Hz	3.27, *m*
[Au(Gly-L-His-N_A,N_P,*N3*)Cl]Cl·3H_2O (**1a**)	8.56 **(-0.06)**	7.31 **(0.00)**	4.01, *dd*, *J* = 17.0, 3.8 Hz **(+0.17)**			4.72, *t*, *J* = 4.0 Hz **(+0.05)**	3.12, *dd*, *J* = 15.8, 4.3 Hz 3.60, *dd*, *J* = 15.8, 4.3 Hz **(+0.09)**
			AlaαCH	**AlaβCH_3**		**HisαCH**	**HisβCH_2**
L-Ala-L-His	8.62	7.31	4.08, *q*, *J* = 7.1 Hz	1.52, *d*, *J* = 7.2 Hz		4.63, *t*, *J* = 7.0 Hz	3.26, *m*
[Au(L-Ala-L-His-N_A,N_P,*N3*)Cl][$AuCl_4$]·H_2O (**2a**)	8.54 **(-0.08)**	7.29 **(-0.02)**	4.13, *q*, *J* = 7.2 Hz **(+0.05)**	1.54, *d*, *J* = 7.2 Hz **(+0.02)**		4.64, *t*, *J* = 4.1 Hz **(+0.01)**	3.12, *dd*, *J* = 15.7, 4.2 Hz 3.57, *dd*, *J* = 15.7, 4.2 Hz **(+0.085)**
			ValαCH	**ValβCH**	**ValγCH_3**	**HisαCH**	**HisβCH_2**
L-Val-L-His	8.63	7.33	3.90, *d*, *J* = 5.6 Hz	2.24, *m*	1.01, *dd*, *J* = 6.6, 3.8 Hz	4.57, *t*, *J* = 6.8 Hz	3.26, *m*
[Au(L-Val-L-His-N_A,N_P,*N3*)Cl]Cl·2H_2O (**3**)	8.55 **(-0.08)**	7.29 **(-0.04)**	3.98, *d*, *J* = 3.3 Hz **(+0.08)**	2.35, *m* **(+0.11)**	1.05, *dd*, *J* = 19.1, 7.1 Hz **(+0.04)**	4.65, *t*, *J* = 3.8 Hz **(+0.08)**	3.10, *dd*, *J* = 15.9, 4.0 Hz 3.57, *dd*, *J* = 15.9, 4.0 Hz **(+0.075)**
			LeuαCH	**LeuβCH_2** **LeuγCH**	**LeuδCH_3**	**HisαCH**	**HisβCH_2**
L-Leu-L-His	8.63	7.32	4.00, *t*, *J* = 7.0 Hz	1.68, *m*	0.93, *dd*, *J* = 6.4, 1.6 Hz	4.62, *t*, *J* = 7.0 Hz	3.28, *m*
[Au(L-Leu-L-His-N_A,N_P,*N3*)Cl]Cl (**4a**)	8.55 **(-0.08)**	7.30 **(-0.02)**	4.08, *t*, *J* = 6.8 Hz **(+0.08)**	1.80, *m* **(+0.12)**	0.97, *t*, *J* = 5.9 Hz **(+0.04)**	4.67, *t*, *J* = 4.0 Hz **(+0.05)**	3.12, *dd*, *J* = 16.1, 4.1 Hz 3.58, *dd*, *J* = 15.1, 3.4 Hz **(+0.07)**

IR and UV-vis characterization. The IR and UV-vis spectroscopic data for the gold(III) complexes with L-histidine-containing dipeptides are listed in the Experimental section (*vide infra*) and are consistent with the structural formula presented in Scheme 1. The IR spectra of these complexes recorded in the range of 4000 – 450 cm^{-1} show the peaks that are attributed to the coordinated X-L-His dipeptides. The coordination of the dipeptides through the amino group of the N-terminal amino acid leads to the disappearance of the bands in the range of 1660 – 1590 and 1550 – 1480 cm^{-1} which are

View Article Online
DOI: 10.1039/C6DT04862E

due to the antisymmetric and symmetric bending vibrations of the NH_3^+ group in zwitterion form. The amide fragment bands in the IR spectra of the uncoordinated dipeptides are found to be at ~ 3200 cm^{-1} (ν_{NH}), in the 1690 – 1640 cm^{-1} region ($\nu_{C=O}$, amide I) and at ~ 1550 cm^{-1} (δ_{NH}, amide II).[35] However, the bands assigned to stretching and bending modes of NH group are absent in the IR spectra of the gold(III) complexes, indicating that coordination of the Au(III) ion to the amide nitrogen was accompanied by its deprotonation. Moreover, the coordination of the deprotonated amide nitrogen results in the shifting of amide I $\nu_{C=O}$ frequencies to the lower values with a difference within 19 – 67 cm^{-1} compared to the free ligands (at 1691, 1659, 1669 and 1670 cm^{-1} for Gly-L-His, L-Ala-L-His, L-Val-L-His and L-Leu-L-His, respectively). Finally, the presence of the strong bands in the range of 1750 – 1700 cm^{-1} in the IR spectra of the complexes are due to the antisymmetric stretching vibrations of C=O in the protonated carboxyl group,[36] and additionally confirms that the oxygen atom of this group does not participate in the coordination with Au(III) ion.

The shape of the UV-vis spectra and values of λ_{max} are almost identical for all investigated complexes, indicating the same coordination mode of X-L-His dipeptides. The absorption around 280 nm observed for the complexes corresponds to LMCT (ligand-to-metal charge transfer) transitions.[37] The intensity of absorption maxima for complexes **2a** and **4b** is approximately twice as high as for the other investigated gold(III)-peptide complexes, which can be attributed to the presence of $[AuCl_4]^-$ counter anion in the crystals of these two complexes.

Crystallographic characterization of the gold(III) complexes with L-histidine-containing dipeptides

Composition of the complexes. The X-ray crystal structure analysis of the complexes **2a**, **3**, **4a** and **4b** allowed us to establish the content of the samples and to perform full structural characterization of the homologous series of the gold(III) complexes with L-histidine containing dipeptides by comparing the obtained results with the available literature data for complexes **1a**, **1b** and **2b**,[19,20] taking into account the influence of the counter anion and water molecules. As far as the composition of the samples is concerned, the most obvious difference between the gold(III) complexes with Gly-L-His and L-Ala-L-His peptides on one side, and L-Val-L-His and L-Leu-L-His on the other side is that we have not been able to incorporate the nitrate groups as the counter ions into the crystal lattice of the latter two complexes. Another unexpected effect is an appearance of tetrachloridoaurate(III) salts of $[Au(L\text{-}Ala\text{-}L\text{-}His\text{-}N_A,N_P,N3)Cl]^+$ and $[Au(L\text{-}Leu\text{-}L\text{-}His\text{-}N_A,N_P,N3)Cl]^+$ complexes instead of the expected nitrate and chloride salts. Complex **3** crystallizes with two symmetry independent, though geometrically similar, structural units (Z'=2), while the other three crystals (**2a**, **4a** and **4b**) contain one formal molecule in the asymmetric part of the unit cell (Z'=1).

Environment of the Au(III) ion in complex cations. In principle the Au(III) ion has coordination number four, which however, in **2a** and **4b** is extended to five, and in **3** to six by weak Au···Cl interactions (*vide infra*). Au(III) ion is bound to one dipeptide molecule *via* three nitrogen atoms of the amino, peptide and imidazole groups. The fourth bond joins the Au(III) ion to the chloride ligand. This is illustrated for the newly investigated complexes **2a**, **3**, **4a** and **4b** in Fig. 1. The bond lengths and angles for these complexes are shown in Table S1, which also lists the corresponding parameters in comparable structures, *i.e.* **1a**,[19] **1b** and **2b**.[20] The Au—N bonds have lengths in the range of 1.91(1) to 2.03(1) Å with no particular distinction to which of the three nitrogen atoms they are formed. The angle N1—Au1—N2 (within the five-membered ring) has values in the range from 80.8(4) to 84.8°, while the one within the six-membered ring *i.e.* N3—Au—N2 spreads the values from 90.9 to 95.7(4)°. It is important to note that the numbering of the atoms used in this section does not match the one applied in the NMR studies, reported above. Marked deviations in angles around the metal from the ideal 180° valence angle are more severe for N2—Au1—Cl1 than for N1—Au1—N3, covering the range from 171.7(2) to 174.7(3)°. This angle involves a peptide nitrogen which is a member of six- and five-membered chelate rings, so the smaller than expected value for this angle, might be the result of the requirement that the three bonds around the peptide nitrogen remain approximately coplanar. The peptide groups C1—C2—O1—N2—C3, the imidazole groups C5—C6—N4—C7—N3, and the carboxyl groups C3—C8—O2 and O3 are planar within the limits of accuracy. The five-membered chelate rings —Au—N1—C1—C2—N2— in **1a** and **4a** complex cations are planar (see Table S2 for a list of endocyclic torsion angles). They become somewhat puckered in two independent molecules of **3** (the average endocyclic torsion angle moduli |ω|being equal to 10.8(4.4) and 11.5(5.6)°, respectively) with the peptide nitrogen atom deviating the most from the ring main plane. Within a series of chloride salts (**1a**, **3** and **4a**) the slight increase of the ring puckering in **3** and its absence in **4a** might mirror a difference in steric hindrance between the bulky isopropyl group directly bonded to C1 (**3**) or bonded to C1 *via* the methylene bridge (**4a**), but it may well result from an engagement of the complex cations of **3** in self-assembly by means of Au···Cl interactions *(vide infra*). In contrast to the chloride salts **1a**, **3** and **4a**, in which the five-membered chelate ring is planar or nearly so, the nitrate salts **1b** and **2b**[20] display the most puckered five-membered chelates, where the average endocyclic torsion angle moduli span the values of 13.1(4.9), 17.1(9.2) and 20.3(7.9)° (three independent observations) and with either Au1 or both Au1 and N1 deviating from the ring main plane. In the tetrachloridoaurate(III) salts **2a** and **4b**, the degree of the five-membered chelate ring puckering is intermediate between the two discussed extremes with the average torsion angle moduli of 9.8(4.5) and 14.6(6.3)°, respectively. Noticeably higher ring puckering in **4b** compared with **2a** illustrates the effect of the replacement of the C1-metyl group by the *iso*-butyl substituent. Taken together, it looks as though planarity of the five-membered chelate ring in the investigated series of structures not only depends on the substitution on C1, which is to be expected, but also, to even bigger extent, on the type of

DOI: 10.1039/C6DT04862E

the counter anion and imposed by it the mode of association of the complex cations in crystals. The conformation of the six-membered chelate rings is described in terms of the endocyclic torsion angles listed in Table S2. The conformation is highly distorted from any of the ideal forms. In majority of structures, it can best be described as 1,3-diplanar with the histidine C*α* and C*β* below and above the plane defined by the remaining atoms. However, in some structures (one of the two independent molecules of **1b**), the ring approaches a sofa conformation with the histidine C*β* (C4 according to the crystallographic numbering scheme) out of the plane of the other five atoms. The angle between the planes of the imidazole ring and the coordination square takes the values from 6.3(4) to 24.8°. The carboxyl group adopts an axial orientation with respect to the coordination plane and the plane of the carboxyl group (C-COO) forms angles in the range from 76.8(4) to 89.1° and from 59.4(5) to 82.0(3)° with the planes of the coordination square and the imidazole group.

Environment of the Au(III) ion in tetrachloridoaurate(III) anion. Bond lengths within the tetrachloridoaurate(III) anion well mirror the engagement of particular chlorine atoms in intermolecular interactions. The involvement in multiple intermolecular interactions leads to significant lengthening of the Au—Cl bond. This is exemplified by Au—Cl2 and Au—Cl5 bond lengths in crystals of **2a** which measure 2.294(3) and 2.283(3) Å, while the remaining two bonds are 2.267(3) and 2.262(3) Å. Similarly, in the crystal of **4b**, the Au—Cl bond lengths to chlorine atoms involved in intermolecular interactions are 2.270(2), 2.280(3) and 2.283(3) Å, while the analogous bond to the chlorine atom that does not participate in intermolecular interactions is much shorter (2.258(3) Å). Such clear correspondence between bond lengths and intermolecular interactions is rarely observed, as the change of the bond length requires relatively high energy expenditure.

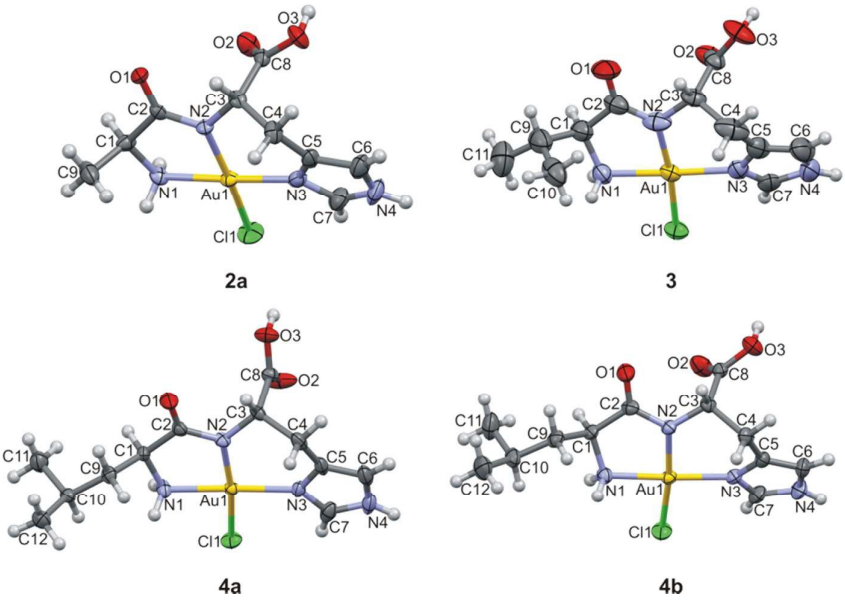

Fig. 1 Ellipsoid representation of complex cations present in the crystals of **2a**, **3** (one of two crystallographically independent molecules), **4a** and **4b.** Displacement ellipsoids are drawn at 40% probability level. The hydrogen atoms are presented in an arbitrary scale.

The role of the particular functional groups in intermolecular interactions. Geometrical parameters describing hydrogen bond interactions in seven crystal structures of gold(III) complexes with L-histidine-containing dipeptides are presented in Table S3. Because of the presence of the L-histidine residue in all investigated crystal structures, the involvement of imidazole ring in hydrogen bonding might be of special interest. It appears that both N-H and C-H donors are engaged in hydrogen bonding. Most remarkable is a short C-H···O hydrogen bond from C7-H to the peptide or carboxylate C=O, which supports the self-association of cationic species. Meanwhile, the N-H(imidazole) functionality is nearly always utilized for the purpose of communication with the anionic species, the only exception being the highly hydrated complex **1a**, in which the imidazole nitrogen acts as a hydrogen bond donor to one of the water molecules.

Having two hydrogen bond donor groups, the amine group utilizes at least one of them to bind to a counter ion and/or to a water molecule. If the other hydrogen atom is used for the self-assembly of the complex cationic species, it binds to a peptide (**1b**, **2a**) or to a carboxyl C=O group (**4a**). This type of peptide-peptide interactions is seen in the docking studies described below.

The carboxyl group preferentially binds to water molecules by utilizing either its proton donor or proton acceptor ability or both. In non-hydrated species, it donates hydrogen bonds to the counter anions (Cl^- or NO_3^-). However, the H-bond donation to the nitrate group forces the carboxyl group to

View Article Online
DOI: 10.1039/C6DT04862E

change its conformation from the preferred *syn* to *anti*, which is rare in crystal structures containing the carboxyl functionality.[20] Only in [Au(L-Leu-L-His-N_A,N_P,*N3*)Cl]$^+$ complexes (**4a** and **4b**), the carboxyl group is being utilized in self-assembly of the cationic species, either as a hydrogen bond donor to a peptide carbonyl group (**4b**) or as a hydrogen bond acceptor from the amine NH functionality (**4a**), again resembling the peptide-peptide interactions seen in the docking studies (*vide infra*).

As one can observe in the non-hydrated crystals of **4a**, the peptide carbonyl group may be excluded from the process of formation of strong intermolecular hydrogen bonds, presumably due to the lack of the sufficient amount of the hydrogen bond donor groups. Instead, the group is involved in weak both inter- and intramolecular hydrogen bonds that involve CH groups as donors. The intramolecular C*-H···O(=C) hydrogen bond (2.32 Å, 2.728(9) Å and 104° for H···O, C···O and C-H···O, respectively) can also be classified as CH/CO dipolar interaction, where the pseudo-torsion angle between the pair of the C*-H/C=O dipoles situated in respective 1,3-positions amounts to 18°. In the remaining crystal structures, deprived of this type of dipolar interactions, the pseudo-torsion angle between the two dipoles adopts much higher values, which cover the range from 27 to 42°. Characteristics of Au(III) complexes with chloride ligands are the Au···Cl intermolecular interactions that usually supplement the square-planar coordination around the Au(III) cation to five or six. As mentioned previously, this kind of interactions, although weak, was present in the crystal structures of nitrate salts (**1b** and **2b**).[20] In these crystals the Au···Cl interactions, formed between the complex cations, extended through the entire crystal in a form of chain or ladder motifs. It may look as though the presence of the tetrachloridoaurate(III) anion, possessing four Au—Cl bonds, increases a chance for the occurrence of the Au···Cl interactions. They are indeed present and quite strong in the crystals of the tetrachloridoaurate(III) salts **2a** and **4b** but, unlike in the nitrate salts, they act between pairs of complex cations and anions, extending the coordination number of Au(III) to five. These discrete Au···Cl interactions gain additional support from the amine NH group, which is engaged in NH···Cl hydrogen bonding to one of the chloride atoms of the same tetrachloridoaurate(III) complex anion that is involved in Au···Cl interactions with the complex cation (Fig. 2). In **2a**, the Au···Cl contacts measure 3.496(3) and 3.284(2) Å, while in **4b**, a single Au···Cl distance amounts to 3.371(3) Å. These values can be compared with the sum of the van der Waals radii for Au and Cl atoms equal to 3.41 Å.[38] In dihydrated crystals of **3**, two symmetry independent complex cations associate with Au···Cl interactions that extend through the entire crystal forming a ladder motif and supplement the square-planar coordination around Au(III) to an elongated tetragonal octahedron. This is illustrated in Fig 3. Interestingly, this kind of interaction is absent in the crystals of other chloride salts of gold(III) complexes with either Gly-L-His (**1a**) or L-Leu-L-His (**4a**) dipeptides, but has been observed in all crystal forms of the nitrate salts of gold(III) complexes with Gly-L-His (**1b**) and L-Ala-L-His (**2b**).[20] In the crystals of **3**, the Au1···Cl2 contacts amount to 3.533(2) and 3.456(2) Å, while the analogous Au2···Cl1 distances are 3.436(2) and 3.595(2) Å. Notably, crystals of **3** display the biggest variety of intermolecular interactions. Besides the already mentioned Au···Cl interactions and the various types of hydrogen bonds, in these crystals there are π···π interactions between pairs of parallel imidazole rings belonging to the symmetrically independent molecules. The two rings are inclined at an angle of 6.9(4)° and the distance between the gravity centers of the two rings amounts to 3.38 Å.

Water molecule is by all means a mediator. For example, in **2a** it bridges two distant amine and carboxyl groups of the same complex cation by engaging to this process the peptide oxygen from the neighboring molecule. Simultaneously, by accepting a hydrogen bond from another complex cation the water molecule mediates in joining together solely the complex cations. But much more often, if present in the crystal lattice, water molecule mediates in joining together the cationic and anionic species. In the absence of crystalline water molecules (**4a**), the complex cations utilize the proton donor properties of amine, carboxyl and NH-imidazole to link all these functionalities to a single counter ion.

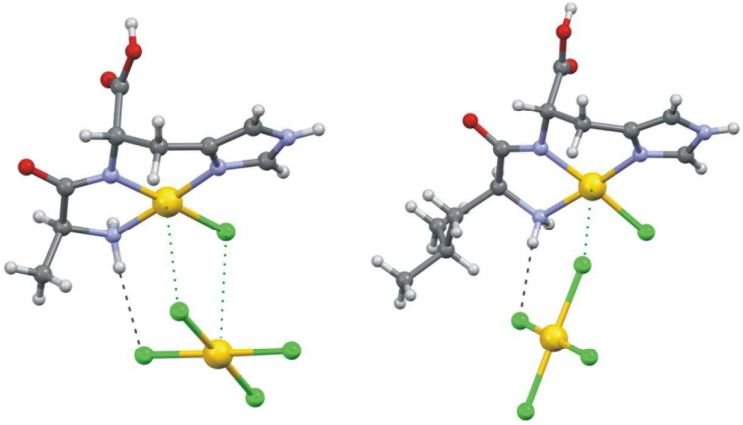

2a 4b

View Article Online
DOI: 10.1039/C6DT04862E
Journal Name ARTICLE

Fig. 2 Pairwise and single Au···Cl interactions between complex cations and anions in crystal structures of **2a** and **4b**, respectively, supported by NH···Cl hydrogen bonds.

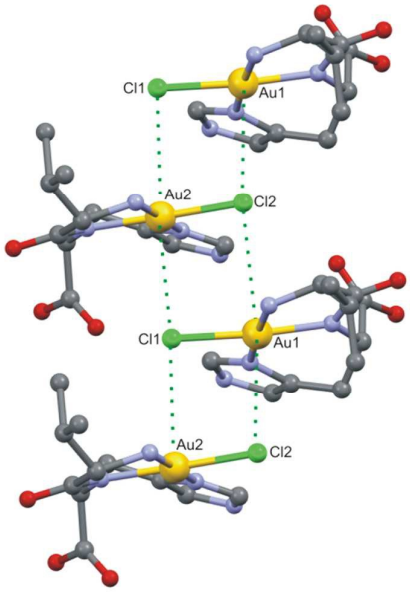

Fig. 3 The arrangement of Au···Cl dipoles (represented as balls and sticks) into a ladder motif in the crystal of **3**. Hydrogen atoms have been omitted for clarity.

Biological activity of the gold(III) complexes with L-histidine-containing dipeptides

Antimicrobial and cytotoxic activity. Prompted by the recent reports of efficient and broad-spectrum antimicrobial activity of auranofin[28,29] and various gold(I) and gold(III) complexes,[39] we have examined the antimicrobial potential of the synthesized gold(III) complexes with L-histidine-containing dipeptides. The antimicrobial activities of the gold(III) complexes with L-histidine-containing dipeptides X-L-His (X = Gly, L-Ala, L-Val and L-Leu), namely **1a**, **1b**, **2a**, **2b**, **3**, **4a** and **4b**, the starting $K[AuCl_4]$ and auranofin were evaluated against the broad panel of Gram-positive (*Staphylococcus aureus*, *Lysteria monocytogenes, Enterococcus faecalis* and *Enterococcus faecium*) and Gram-negative (*Acinetobacter baumannii*) bacteria and two strains of *Candida* (*C. albicans* and *C. parapsilosis*), while their cytotoxic properties were evaluated against one normal (MRC5, human lung fibroblasts) and two cancer cell lines (HeLa, human cervix cancer, and A549, human lung cancer) (Table 2).

While the antibacterial activity was confirmed for the auranofin with MIC (minimal inhibitory concentration) values between 1-10 μM, the most MIC values of the gold(III) complexes with L-histidine-containing dipeptides were between 200 and 400 μM, indicating their moderate to low activity. However, **1b** and **4b** exhibited MIC of 80 μM against Gram-positive *E. faecium* and 100 μM against Gram-negative *A. baumannii* (Table 2). The obtained results were in agreement with our recent study related to the antimicrobial potential of a series of gold(III) complexes differing in the ligand structure, *i.e.* [HGly-Met sulfoxide][$AuCl_4$] (Gly-Met is dipeptide glycyl-methionine), [Au(en)Cl_2]Cl·$2H_2O$ (en is ethylenediamine), [Au(dien)Cl]Cl_2 (dien is diethylenetriamine), [Au(Gly-L-His-N_A,N_P,*N3*)Cl]NO_3·$1.25H_2O$ (complex **1b** in the present study), [Au(L-Ala-L-His-N_A,N_P,*N3*)Cl]NO_3·$2.5H_2O$ (complex **2b** in the present study) and [Au(Gly-Gly-L-His-N_A,N_{P1},N_{P2},*N3*)]Cl·H_2O (Gly-Gly-L-His is tripeptide glycyl-glycyl-L-histidine), also showing that two gold(III) complexes with L-histidine-containing dipeptides exhibited relatively weak effects compared to the others against the investigated bacterial strains, both ATCC and clinical isolates.[40] The $K[AuCl_4]$ was the most active against *S. aureus* (MIC = 80 μM) and exhibited similar antibacterial activity to that of the investigated gold(III) complexes (Table 2). In the case of the fungi, *C. parapsilosis* was more sensitive to the investigated gold(III) complexes in comparison to *C. albicans*; nevertheless, all MIC values against the fungi were relatively high, except the ones for auranofin (MIC = 10 μM). Greater sensitivity of *C. parapsilosis* may be of some interest, as this strain had shown steady incline in prevalence, causing severe infections in neonates and patients in intensive care units.[41] Under the tested conditions, none of the L-histidine-containing dipeptides was toxic towards the investigated strains in concentrations up to 500 μM.

Table 2 Antimicrobial activity expressed as MIC (μM)[a] and cytotoxic activity expressed as IC_{50} value (μM)[b] for all gold compounds used in this study. L-Histidine-containing dipeptides had no observable activities at concentrations > 500 μM.

Complex	1a	1b	2a	2b	3	4a	4b	$K[AuCl_4]$	Auranofin
Microorganism									
S. aureus NCTC 6571	300	300	200	400	400	300	300	80	5
L. monocytogenes NCTC 11994	200	200	100	200	200	200	200	100	10
E. faecalis ATCC 29212	200	200	200	200	200	200	200	200	1.25
E. faecium ATCC 6057	200	80	200	200	200	200	80	200	2.5
A. baumannii ATCC 19606	100	100	100	100	100	200	100	100	2.5
C. albicans ATCC 10231	400	500	400	400	500	200	400	100	10
C. parapsilosis ATCC 22019	200	200	200	400	400	100	200	200	10
Cell line									

View Article Online
DOI: 10.1039/C6DT04862E

MRC5	> 200	> 200	150	> 200	> 200	170	100	150	0.9
HeLa	150	> 200	75	170	> 200	55	65	170	0.5
A549	150	> 200	30	170	> 200	115	75	160	0.5

[a]The MIC values were determined in duplicates in three independent experiments. SD were within 2-5%.
[b]IC_{50} is defined as the concentration inhibiting 50% of cell growth after the treatment with the test compounds. Results are from three independent experiments, each performed in quadriplicate. SD were within 2-5%.

Like in this study, only moderate activity against bacteria and fungi was found for the organometallic gold(III) thiosalicylate complex,[42] as well as for most of the organogold(III) complexes containing imidate[43] and *bis*(amidate) ligands.[44] On the other hand, mononuclear gold(III) complexes with aromatic nitrogen-containing heterocycles of the general formula $[AuCl_3(N\text{-heterocycle})]$ (N-heterocycle is pyridazine, pyrimidine, pyrazine, quinoxaline and phenazine)[45] and dinuclear $\{[AuCl_3]_2(\mu\text{-L})\}$ complexes (L stands for 4,4'-bipyridine and 1,2-bis(4-pyridyl)ethane)[46] exhibited slightly better activity against the investigated bacterial and fungal strains than the presently investigated gold(III)-dipeptide complexes. Moreover, organometallic complexes $[AuCl_2(damp)]$, $[Au(CH_3COO)_2(damp)]$ and $[AuCl_2(ppy)]$ (damp is 2-((dimethylamino)methyl)phenyl and ppy is 2-pyridylphenyl) showed a broad-spectrum and good to excellent antimicrobial activity against different strains, with some preference for Gram-positive bacteria, *S. aureus* and *E. faecalis*.[47,48]

Rationale behind the numerous efforts to develop cytotoxic agents based on gold(III) is the fact that Au(III) ion is isoelectronic with Pt(II), and its complexes usually adopt the square planar geometry similar to the clinically utilized platinum-based agents cisplatin and carboplatin.[49,50] Surprisingly, most of the studied gold(III) complexes showed modest binding activity to double stranded DNA, and exhibited relatively high reactivity towards various proteins.[51,52] Our present results confirm the cytotoxic potential of auranofin with IC_{50} values in accordance to the previous studies on the same cell lines.[53] However, the cytotoxic effect of the most active of the studied gold(III) complexes with L-histidine-containing dipeptides, **2a**, was from 60 to 170-fold lower in comparison to that of auranofin, for A549 and MRC5 cell lines, respectively (Table 2). Complexes **3** and **1b** exhibited no detectable toxicity in concentrations up to 400 μM and thus their IC_{50} values were denoted as > 200 μM (Table 2). Complexes **2a, 2b, 4a** and **4b** showed some selectivity between the normal fibroblasts MRC5 and human cervical cancer (HeLa) and adenocarcinomic human alveolar basal epithelial cells (A549). Lower cytotoxic effects or their complete lack are actually in line with the comparable studies, where **1a** was reported to exhibit cytotoxic effect upon prolonged exposure of 72 h with ovarian carcinoma cell line A2780/S and A2780/R (IC_{50} of 5.2 and 8.5 μM) and IC_{50} values of more than 120 μM upon shorter exposure times.[24] Furthermore, IC_{50} values determined for gold(III)-dipeptide complexes are similar to the ones reported for $[Au(dien)Cl]Cl_2$ and $[Au(cyclam)](ClO_4)_2Cl$ (cyclam is 1,4,8,11-tetraazacyclotetradecane) from the systematic study conducted on the panel of 12 cell lines.[52] It is worth mentioning that the $[Au(dien)Cl]Cl_2$ complex has the same N_3Cl coordination sphere as the complexes presently investigated, while in the $[Au(cyclam)](ClO_4)_2Cl$, the corresponding ligand is coordinated to Au(III) ion through four nitrogen atoms. Moreover, similar to our study, a negligible cytotoxicity on the A549 cell line was previously observed for $[Au(bipy^{dmb}\text{-}H)(OH)][PF_6]$, $[Au(bipy^{dmb}\text{-}H)(2,6\text{-xylidine-H})][PF_6]$, $[Au(bipy^{dmb}\text{-}H)(p\text{-toluidine-H})][PF_6]$ ($bipy^{dmb}$ = 6-(1,1-dimethylbenzyl)-2,2'-bipyridine), $[Au(py^{dmb}\text{-}H)(AcO)_2]$ (py^{dmb} = 2-(1,1-dimethylbenzyl)-pyridine) and $K[Au(pz^{Ph}\text{-}H)Cl_3]$ (pz^{Ph} = 1-phenylpyrazole) complexes with IC_{50} values ≥ 35 μM.[54] On the other hand, gold(III) complexes containing dithiocarbamates, $[Au(dmdt)Cl_2]$, $[Au(dmdt)Br_2]$ (dmdt = *N,N*-dimethyldithiocarbamate), $[Au(esdt)Cl_2]$ and $[Au(esdt)Br_2]$ (esdt = ethylsarcosinedithiocarbamate), have been proved to be very active on the HeLa and A549 cell lines, with IC_{50} values falling in the low micromolar or even nanomolar range.[55]

Overall, gold(III) complexes with L-histidine-containing dipeptides are not potent antimicrobials and do not have great anticancer potential, however their low cytotoxicity towards normal cell line makes them suitable candidates for further examination towards other activities including antiinflammatory, antiangiogenic or for utilization in the combination therapy. Therefore, complexes that did show some antimicrobial properties and selectivity in terms of cancer *vs.* normal cell lines (**2a**, **2b**, **4a** and **4b**) were brought forward for *in vivo* studies on zebrafish embryo model.

Embryotoxicity and antiangiogenic potential. Zebrafish is recognized as a reliable and versatile *in vivo* platform for early drugs' safety evaluation.[56] The *in vivo* toxicity assessment performed in this study showed that gold(III) complexes with L-histidine-containing dipeptides **2a**, **2b**, **4a** and **4b** were markedly less toxic (lethal and teratogenic) to zebrafish embryos in comparison to auronofin, ranking them as follow: auranofin > **2a** > **$K[AuCl_4]$** > **2b** > **4b** > **4a.** Based on the determined LC_{50} concentration values, auranofin was between 3 and 33-fold more toxic in comparison to the gold(III) complexes **2a** and **4a,** respectively (Fig. 4). Our results confirmed the embryotoxicity of auranofin in accordance with the previous studies on zebrafish embryos model,[57,58] showing serious cardiovascular and skeletal defects in the embryos exposed to doses ≥ 2.5 μM, and 100% mortality rate of the embryos at doses ≥ 7.5 μM during 114 h treatment (Fig. 4). On the other side, embryos treated with gold(III) complexes had no developmental defects at doses up to 100 μM, except for the case of **2a** treatment. Complex **2a**, although with the lowest LC_{50} of 11.6 μM, caused pericardial edema in embryos at each of tested concentrations, which survived up to 114 hpf (hours post fertilization). Complexes **2b** and **4b** had comparable LC_{50} concentration values of close to 60 μM, while $K[AuCl_4]$ was more toxic (LC_{50} = 47 μM) than **2b**, **4a** and **4b**, and without adverse developmental effects. Interestingly, embryos upon treatment with each of the complexes had reduced or

View Article Online
DOI: 10.1039/C6DT04862E
Journal Name ARTICLE

absent caudal circulation, similarly to the pattern observed in embryos upon auranofin treatment. These complex-treated embryos had neither developmental defects (except of those treated with **2a**) nor body necrosis, which develops upon treatment with auranofin (Fig. 4). It has been observed that complexes **2a**, **4a** and **4b** interfered embryos hatching, like auranofin, but with different final outcome (Fig. 4). While auranofin-treated embryos have already been prevented for hatching at 2.5 μM and all unhatched embryos died up to 114 hpf, the unhatched embryos upon tested concentrations range of **2a** (12.5 - 100 μM) survived up to 114 hpf. On the other hand, **4a** and **4b** inhibited embryos hatching only at ≥ 50 μM, where all unhatched embryos upon **4a** treatment survived up to 114 hpf without observable deformities and cardiovascular defects, while majority of those upon **4b** died in a period between 96 hpf and 114 hpf (Fig. 4). In comparison to the corresponding LC_{50} values of gold(III) complexes with aromatic nitrogen-containing heterocycles that have previously been addressed in the zebrafish embryos,[45] gold(III) complexes with L-histidine-containing dipeptides explored in this study showed up to 5.2-fold less toxicity. Inhibition of embryos hatching has been observed for both groups of gold(III) complexes, suggesting that observed effect on the hatching may be attributed to the Au(III) ions. Recently, Lin et al.[59] demonstrated that some free metal ions released from metal-oxide nanoparticles could bind to the active site of Zn-metalloproteases, enzymes involved in the hatching process, and thus may inhibit their activity and hatching success.

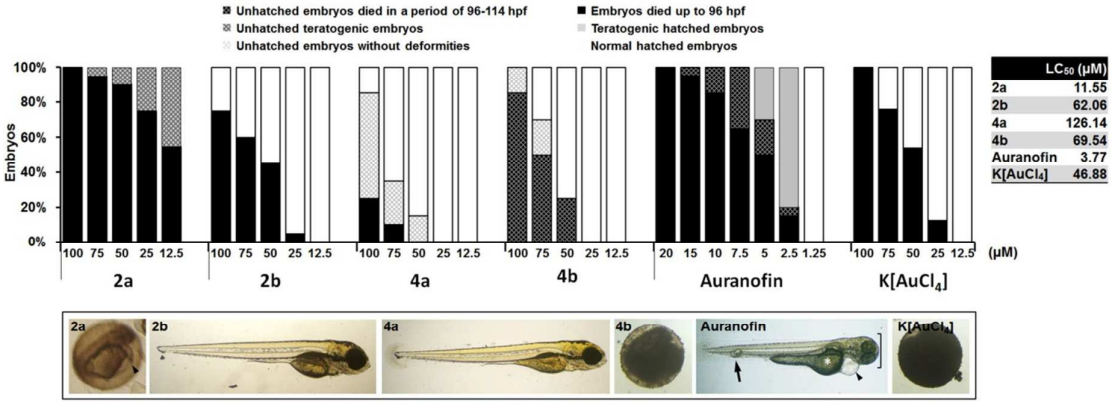

Fig. 4 Results of the toxicity assay on zebrafish embryos exposed to gold(III) complexes **2a, 2b, 4a** and **4b**, $K[AuCl_4]$ and auranofin expressed as LC_{50} values (μM). Morphology of zebrafish embryos at 114 hpf after treatment with 75 μM of **2a** (unhatched teratogenic), **2b** (normal), **4a** (normal), **4b** (unhatched embryos dead in a period from 96-114 hpf), $K[AuCl_4]$ (dead) and 7.5 μM of auranofin (teratogenic) are shown. Dipeptides L-Ala-L-His and L-Leu-L-His had no toxic activity on zebrafish embryos at concentration up to 200 μM. Embryos upon 75 μM of **2a** developed pericardial edema (arrowhead), while embryos upon 7.5 μM of auranofin were retarded in the growth, had small head with malformed eyes (bracket), large pericardial edema (arrowhead), non-resorbed egg yolk (asterisk) and necrotic tissue in the tail region (arrow).

Based on our recent study on gold(III) complexes with 1,7- and 4,7-phenanthroline,[60] and the pattern of reduced caudal circulation observed during the embryotoxicity assessment, we have decided to examine the ability of gold(III) complexes with L-histidine-containing dipeptides to affect angiogenesis *in vivo* in the zebrafish model. Angiogenesis plays an essential role in many physiological and pathological conditions including inflammatory diseases such as rheumatoid arthritis, psoriasis and cancer.[61] It is defined as process of formation of new blood vessels from the preexisting ones,[62] and thioredoxin reductase (TrxR) has been implicated in this process.[63] The suppression effect on angiogenesis by complexes **2a**, **2b**, **4a** and **4b** has been verified *in vivo* using transgenic zebrafish [*Tg*(*fli-1*:*EGFP*)] embryos, in which the endothelial cells expressing EGFP can be directly observed by fluorescence microscope.

The developmental angiogenesis in zebrafish embryos, leading to the formation of the intersegmental vessels (ISVs) at 48 hpf, and subintestinal vessels (SIVs) at 72 hpf, represents a target for the screening of antiangiogenic compounds.[64] The embryos upon treatment with different gold(III) complexes displayed different antiangiogenic phenotypes, while 0.1% DMSO and corresponding ligands had no effect on the formation of ISVs and SIVs which were developed as a basket-like structure with 5 - 9 arcades (Fig. 5 and Fig. S1). The starting $K[AuCl_4]$ complex at 35 μM concentration had only weak effect on SIVs sprouting, while did not affected ISVs development. In the auranofin (1.25 μM) and sunitinib malate (1.25 μM) treated groups, that are known for their antiangiogenic activities, SIVs formation was almost totally inhibited, while some ISVs were defective or absent. In both cases, treated embryos suffered from serious pericardial edema (Fig. 5). The inhibition of SIVs formation was achieved by each of four gold(III)-dipeptide complexes in the dose-dependent manner, whereas 35 μM of **2a** and **4b** almost completely inhibited their development (Fig. S1).

Reduced ISVs and disrupted dorsal longitudinal anastomotic vessels (DLAV) have been detected upon **2a** (35 μM) treatment, while **2b** treated embryos showed thinner ISVs (Fig. 5). Embryos treated with 35 μM of **4a** and **4b** had markedly thinner ISVs then 0.1% DMSO-treated ones, and interrupted DLAV in some segments. Most of embryos possessing thinner ISVs had very slow (upon 25 μM treatments) or totally absent (upon 35 μM treatments) blood

View Article Online
DOI: 10.1039/C6DT04862E

circulation in the caudal region indicating that if vessels were initially developed, they were not functional. Notably, none of embryos exposed to complexes **2a**, **2b**, **4a** and **4b** suffered from pericardial edemas neither had disturbed heartbeating rate, as opposed to embryos treated with 1.25 μM auranofin and sunitinib malate (Fig. 4).

Overall, gold(III) complexes with L-histidine-containing dipeptides showed antiangiogenic activity *in vivo* in zebrafish embryos model, where the complexes **2a** and **4b** had the highest antiangiogenic potential. Although gold(III) complexes achieved comparable antiangiogenic effect to auranofin and sunitinib malate at 30-fold higher concentration, zebrafish embryos upon gold(III) complexes treatment had no cardiovascular side effects in comparison to those upon treatment with auranofin and sunitinib malate, as shown in the angiogenesis assay. Moreover, overall embryotoxicity of gold(III) complexes was significantly lower in comparison to auranofin, proposing them to serve as leads for further development towards antiangiogenic drugs.

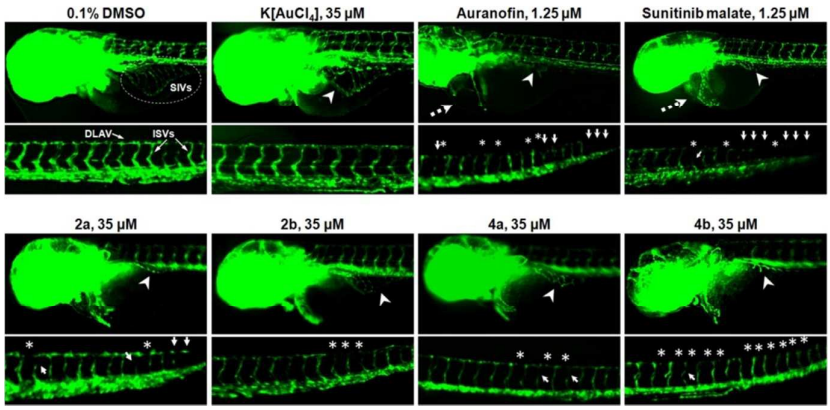

Fig. 5 *In vivo* effect of gold(III) complexes **2a, 2b, 4a** and **4b** in comparison to sunitinib malate (Suten), auranofin and K[$AuCl_4$] on subintestinal vessels (SIVs), intersegmental vessels (ISVs) and dorsal longitudinal anastomotic vessels (DLAV) development in zebrafish embryos assessed at 48 hpf (for ISVs and DLAV) and 72 hpf (for SIVs). Normally developed SIVs, ISVs and DLAV are designated in 0.1% DMSO-treated embryo. Reduced SIVs (arrowhead), disrupted DLAV (asterisk), thinner or reduced ISVs (arrow), and pericardial edema (dashed arrow) are denoted.

Molecular docking study. In the light of recent findings that auranofin and some gold(III) complexes may exert affinity through the inhibition of thioredoxin reductase (TrxR),[29,65] and that this enzyme has been implicated in angiogenesis,[63] we have performed molecular docking study using human and bacterial (*E. coli*) TrxRs as target macromolecules (Fig. 6). The determination of a suitable geometry and binding affinity of the studied complexes (auranofin and cationic part of the gold(III)-dipeptide complexes) to the active site of both receptors was done with the application of the scoring functions.[66] The binding affinities and the energies for the investigated complexes were presented in Table S4. According to the results for HBond, the scoring function that describes hydrogen bond interactions between a given complex and the amino acids from the enzyme active site, for human TrxR the highest interaction was obtained for auranofin, while for *E. coli* TrxR the highest interaction was obtained for **1a/b**. Similarly, according to NoHBond interactions, that are related to the other interactions between complex and amino acids from the enzyme active site, excluding steric and van der Waals interactions, the highest interaction was observed for auranofin and **1a/b** for human and *E. coli* TrxR, respectively. Steric is the scoring function that describes steric interaction between a given complex and the amino acids from the enzyme active site. According to the obtained results for this function, the highest interaction for both human and *E. coli* TrxRs was obtained for auranofin. Furthermore, according to the obtained results for van der Waals interactions between a given complex and the amino acids from the enzyme active site (VdW function), the highest interaction was obtained for **1a**/**b** and auranofin for human and *E. coli* TrxR, respectively. According to the obtained results for the total energy of interactions between the complex and the amino acids from the enzyme active site (energy function), as well as both MolDock and Rerank scores, the highest potency was observed for auranofin for both human and *E. coli* TrxRs. Finally, according to the results for LE1 (complex efficiency defined as MolDock score divided by the heavy atoms count) and LE3 (complex efficiency defined as Rerank score divided by the heavy atoms count), for both human and *E. coli* TrxRs, the highest efficiency was obtained for **1a**/**b.**

The best calculated poses for all studied complexes inside the active site of enzymes are presented in Fig. 6. The best docking pose for each studied complex individually is presented in ESI, as well as two-dimensional representation of their interactions with the amino acids inside the binding pocket of the enzyme with identified hydrogen bonds and hydrophobic interactions between the investigated complexes and amino acids from the enzyme's active site (Fig. S2-S5).

DOI: 10.1039/C6DT04862E

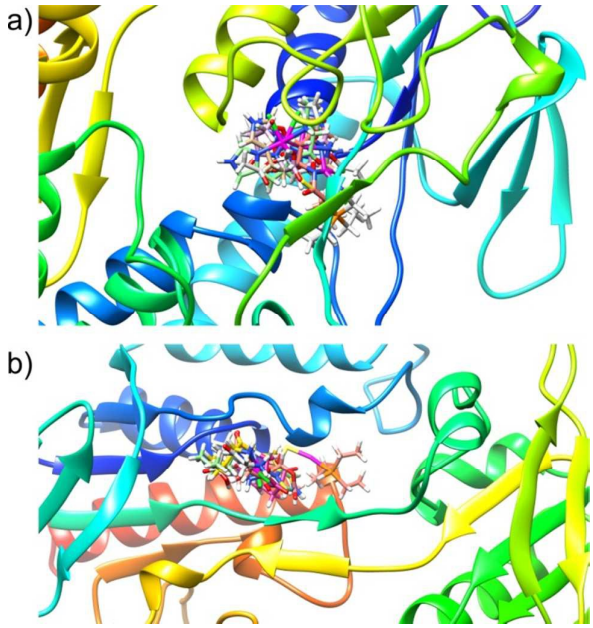

Fig. 6 The best calculated poses for all studied gold(III) complexes and auranofin inside the active site of human **a)** and *Escherichia coli* **b)** thioredoxin reductases.

Conclusions

Seven gold(III) complexes with L-histidine-containing dipeptides were synthesized, structurally characterized by spectroscopy and crystallography and biologically evaluated. In all complexes, dipeptides are tridentate coordinated to the Au(III) ion through the N3 imidazole nitrogen, the deprotonated nitrogen of the amide bond and to the nitrogen of the N-terminal amino group. The presence of Au–Cl dipoles in the crystals creates conditions for their mutual interactions that supplement the square planar coordination around Au(III) to a strongly elongated square pyramid or tetragonal octahedron. These interactions are either isolated, involving pairs of cationic and anionic species, or extend through the entire crystal lattice in a form of chain or ladder motifs consisting solely of cationic species. Particularly suited for the extended Au···Cl dipolar interactions seem to be the nitrate salts. Besides that, the degree of the puckering of the five-membered chelate ring seems to be more associated with the type of the counter anion and the presence of extended Au–Cl dipolar interactions than with the bulkiness of the alkyl substituent at α carbon atom of N-terminal amino acid. Crystals are held together by various types of hydrogen bonds that are usually formed between cationic and anionic species either directly or by means of water molecules. Direct hydrogen bond self-association of cationic species is rarely encountered.

Of a series of the investigated gold(III) complexes, those containing X-L-His dipeptides with X is L-Ala (**2a** and **2b**) and L-Leu (**4a** and **4b**) as N-terminal amino acids turned out to be the most active against the investigated microbial strains and to be selective in terms of cancer *vs.* normal cell lines. Moreover, these four complexes showed antiangiogenic activity *in vivo* in zebrafish embryos, with **2a** and **4b** being the most active. Although these complexes achieved antiangiogenic effect comparable to auranofin and sunitinib malate that are known angiogenic inhibitors, at much higher concentration, zebrafish embryos upon treatment with gold(III) complexes had no cardiovascular side effects. Moreover, overall cytotoxicity and embryotoxicity of **2a, 2b**, **4a** and **4b** were significantly lower in comparison to auranofin, making them good candidates for further development towards antiangiogenic drugs. Finally, all investigated gold(III)-dipeptde complexes have significant interactions with the active sites of both human and *E. coli* thioredoxin reductases, suggesting that main mechanism of their action can be associated with the interaction with this enzyme.

Experimental

Materials

Distilled water was demineralized and purified to a resistance of greater than 10 $M\Omega \cdot cm^{-1}$. The compounds $K[AuCl_4]$, auranofin and D_2O were purchased from Sigma-Aldrich Chemical Co. The dipeptides glycyl-L-histidine (Gly-L-His), L-alanyl-L-histidine (L-Ala-L-His), L-valyl-L-histidine (L-Val-L-His) and L-leucyl-L-histidine (L-Leu-L-His) were obtained from Bachem A.G. All the employed chemicals were of analytical reagent grade and used without further purification.

Measurements

Elemental microanalyses for carbon, hydrogen and nitrogen were performed by the Microanalytical Laboratory, Faculty of Chemistry, University of Belgrade. All pH measurements were made at ambient temperature. The pH meter (S220 SevenCompact™ pH/Ion, Mettler Toledo) was calibrated with buffer solution of pH 4.01. The reported pD values were corrected for the deuterium isotopic effect by adding 0.45 units to the pH meter reading.[67] However, in conceptual references to acidity and basicity, the common symbol pH was used. ^{1}H NMR spectra of gold(III) complexes and L-histidine-containing dipeptides were recorded at 25 ^{o}C in D_2O containing TSP (sodium 3-(trimethylsilyl)propionate) as the internal reference on a Varian Gemini 2000 spectrometer at 200 MHz. Chemical shifts are reported in parts per million (ppm) and scalar couplings are reported in hertz (Hz). 10 mg of each compound was dissolved in 0.7 mL of D_2O, and this solution was transferred into a 5 mm NMR tube. IR spectra were recorded as KBr pallets on a Perkin Elmer Spectrum One spectrometer over the range 4000 – 450 cm^{-1}. The UV-Vis spectra were recorded on a Perkin Elmer Lambda 35 double-beam spectrophotometer equipped with thermostated 1.00-cm quartz Suprasil cells after dissolving the corresponding gold(III) complex in water over the wavelength range of 200 – 600 nm. The concentration of the gold(III)-dipeptide complexes was $5 \cdot 10^{-4}$ M.

View Article Online
DOI: 10.1039/C6DT04862E

Synthesis of gold(III) complexes with L-histidine-containing dipeptides

The gold(III) complexes with L-histidine-containing dipeptides, [Au(Gly-L-His-N_A,N_P,*N3*)Cl]Cl·3H_2O (**1a**), [Au(Gly-L-His-N_A,N_P,*N3*)Cl]NO_3·1.25H_2O (**1b**), [Au(L-Ala-L-His-N_A,N_P,*N3*)Cl][$AuCl_4$]·H_2O (**2a**), [Au(L-Ala-L-His-N_A,N_P,*N3*)Cl]NO_3·2.5H_2O (**2b**), [Au(L-Val-L-His-N_A,N_P,*N3*)Cl]Cl·2H_2O (**3**), [Au(L-Leu-L-His-N_A,N_P,*N3*)Cl]Cl (**4a**) and [Au(L-Leu-L-His-N_A,N_P,*N3*)Cl][$AuCl_4$]·H_2O (**4b**) were synthesized by previously described methods.[19,20] All complexes were pure based on elemental microanalysis and ^{1}H NMR spectroscopy.

0.5 mmol of the corresponding L-histidine-containing dipeptide (106.1 mg of Gly-L-His, 113.1 mg of L-Ala-L-His, 127.1 mg of L-Val-L-His and 134.2 of L-Leu-L-His) was dissolved in 5.0 mL of water and the pH of solution was adjusted to 1.50 - 2.00 by adding 1 M HCl (for **1a**, **2a**, **3** and **4a**) or HNO_3 (for **1b**, **2b**, **3** and **4b**). To this solution was added slowly under stirring an equimolar amount of K[$AuCl_4$] (188.9 mg) dissolved in 3.0 mL of water. The resulting yellow solution was stirred in the dark at room temperature for at least seven days. The Au(0) particles were filtered off and the filtrate was left standing in the dark at room temperature to slowly evaporate to a volume of 3.0 mL. The concentrated solution was then stored in refrigerator and yellow crystals of gold(III) complexes were formed after 3 - 5 days. These crystals were filtered off and dried in the dark at ambient temperature. The yield was 71% (189.3 mg) for **1a**, 68% (179.6 mg) for **1b**, 53% (215.8 mg) for **2a**, 65% (183.5 mg) for **2b**, 56% (156.0 mg) for **3**, 63% (168.6 mg) for **4a** and 52% (222.7 mg) for **4b.**

Anal. calcd. for **1a** ($C_8H_{17}AuCl_2N_4O_6$; M_r = 533.12): C, 18.02%; H, 3.21%; N, 10.51%. Found: C, 17.95%; H, 3.02%; N, 10.28%. IR (KBr, ν, cm^{-1}): 3530(br), 3131, 3098, 3032, 2916(br), 1762(s), 1649(s), 1623(vs), 1495(w), 1474(w), 1430(m), 1397(m), 1336(w), 1313(w), 1285(w), 1256(w), 1205(w), 1181(w), 1166(m), 1117(m), 1065(w), 1041(w), 967(w), 946(w), 854(m), 818(w), 775(w), 630(w), 494(w), 480(w). UV-vis (H_2O, λ_{max}, nm): 277 (ε = 1.7·10^3 $M^{-1}cm^{-1}$).

Anal. calcd. for **1b** ($C_8H_{13.50}AuClN_5O_{7.25}$; M_r = 528.15): C, 18.19%; H, 2.58%; N, 13.26%. Found: C, 18.45%; H, 2.42%; N, 13.08%. IR (KBr, ν, cm^{-1}): 3409(br), 3183, 3120, 3032, 2920(br), 1731(s), 1654(vs), 1527(w), 1507(w), 1426(m), 1384(vs), 1342(m), 1278(m), 1174(s), 1124(m), 1086(w), 1033(w), 980(w), 950(w), 922(w), 853(m), 824(w), 803(m), 699(m), 630(m), 553(w), 505(m). UV-vis (H_2O, λ_{max}, nm): 279 (ε = 1.1·10^3 $M^{-1}cm^{-1}$).

Anal. calcd. for **2a** ($C_9H_{15}Au_2Cl_5N_4O_4$; M_r = 814.43): C, 13.27%; H, 1.86%; N, 6.88%. Found: C, 12.92%; H, 1.80%; N, 6.80%. IR (KBr, ν, cm^{-1}): 3493(br), 3327(m), 3160, 3121, 3003(br), 1697(s), 1592(vs), 1506(w), 1451(w), 1435(w), 1409(m), 1348(w), 1302(w), 1277(m), 1232(m), 1211(m), 1182(m), 1131(w), 1084(w), 1061(w), 1022(w), 977(w), 942(w), 928(w), 879(w), 853(w), 809(w), 788(w), 747(w), 689(m), 620(m), 565(w). UV-vis (H_2O, λ_{max}, nm): 289 (ε = 3.5·10^3 $M^{-1}cm^{-1}$).

Anal. calcd. for **2b** ($C_9H_{18}AuClN_5O_{8.50}$; M_r = 564.70): C, 19.14%; H, 3.21%; N, 12.40%. Found: C, 18.75%; H, 3.18%; N, 12.23%. IR (KBr, ν, cm^{-1}): 3433(br), 3120, 2917(br), 1737(s), 1640(s), 1507(w), 1454(w), 1384(vs), 1298(m), 1188(m), 1114(w), 1084(w), 1014(w), 970(w), 809(w), 630(m), 572(w), 482(w). UV-vis (H_2O, λ_{max}, nm): 289 (ε = 1.1·10^3 $M^{-1}cm^{-1}$).

Anal. calcd. for **3** ($C_{11}H_{21}AuCl_2N_4O_5$; M_r = 557.18): C, 24.50%; H, 3.55%; N, 10.39%. Found: C, 24.29%; H, 3.55%; N, 10.38%. IR (KBr, ν, cm^{-1}): 3402(br), 3114, 3084, 2965, 2862(br), 1728(s), 1644(vs), 1508(m), 1470(m), 1431(w), 1390(s), 1339(m), 1278(m), 1233(m), 1208(s), 1114(w), 1089(m), 1030(w), 996(w), 838(w), 810(m), 779(m), 767(m), 701(w), 659(w), 631(m), 587(w), 501(w). UV-vis (H_2O, λ_{max}, nm): 282 (ε = 1.1·10^3$M^{-1}cm^{-1}$).

Anal. calcd. for **4a** ($C_{12}H_{19}AuCl_2N_4O_3$; M_r = 535.18): C, 26.93%; H, 3.58%; N, 10.47%. Found: C, 27.03%; H, 3.02%; N, 10.46%. IR (KBr, ν, cm^{-1}): 3435(br), 3131(m), 2978, 2924(br), 1722(s), 1646(vs), 1597(m), 1496(m), 1461(m), 1431(m), 1415(m), 1369(s), 1341(m), 1309(w), 1271(m), 1241(m), 1198(s), 1144(w), 1123(w), 1087(m), 1025(w), 1012(w), 971(w), 943(w), 921(w), 856(w), 835(w), 788(m), 675(w), 663(w), 627(m), 583(w), 531(m). UV-vis (H_2O, λ_{max}, nm): 283 (ε = 1.6·10^3 $M^{-1}cm^{-1}$).

Anal. calcd. for **4b** ($C_{12}H_{21}Au_2Cl_5N_4O_4$; M_r = 856.51): C, 16.83%; H, 2.47%; N, 6.54%. Found: C, 16.48%; H, 2.36%; N, 6.47%. IR (KBr, ν, cm^{-1}):~ 3400(br), 3156, 3053, 2962, 2940(br), 1698(s), 1611(vs), 1506(m), 1457(w), 1403(s), 1344(s), 1270(m), 1213(m), 1197(m), 1107(w), 1080(m), 1029(w), 996(w), 963(w), 929(w), 856(w), 823(w), 802(m), 753(w), 669(w), 648(w), 621(m), 580(w), 516(m). UV-vis (H_2O, λ_{max}, nm): 281 (ε = 2.5·10^3 $M^{-1}cm^{-1}$).

Crystallographic data collection and refinement of the structures

Crystals of the complexes **2a**, **3**, **4a** and **4b** suitable for X-ray diffraction analysis were obtained by slow evaporation of water solution in the presence of hydrochloric and nitric acids. The most relevant crystal and refinement data are collected in Table S5. Single crystal X-ray diffraction data were collected on Xcalibur kappa-geometry diffractometer equipped with Eos CCD detector and a graphite monochromated Mo-Kα radiation source (λ = 0.71073 Å) using CrysAlisPro software.[68] Empirical absorption correction using spherical harmonics, implemented in SCALE3 ABSPACK scaling algorithm, was also applied.[69] The structures were solved by direct methods using SHELXS-86[70] and refined by full-matrix least-squares calculations on F^2 with SHELXL-97.[70] Anisotropic displacement parameters were refined for all non-hydrogen atoms. All hydrogen atoms were refined using a riding model with isotropic displacement parameters 20% higher than the isotropic equivalent of their carriers. The positions of the hydrogen atoms attached to the carbon and nitrogen atoms were calculated at standardized

View Article Online
DOI: 10.1039/C6DT04862E

distances (methyl C–H = 0.96, methylene C–H = 0.97, methine C–H = 0.98, aromatic C–H = 0.93, aromatic N–H = 0.86 and amine N–H = 0.89 Å). The water hydrogen atoms were positioned on difference Fourier maps and the O–H distances were standardized to 0.82 Å. The hydroxy hydrogen atoms were positioned using facilities provided by SHELXL-97; HFIX147 at standardized distances (0.82 Å). The absolute structure of the crystals was assumed from the known absolute configuration of the dipeptides used in the synthesis and was confirmed by the Flack parameter.[71] MERCURY[72] program was used to prepare drawings.

Biological activity testing

Evaluation of antimicrobial properties. Gold(III) complexes with L-histidine-containing dipeptides, auranofin and $K[AuCl_4]$ were evaluated against the broad panel of microorganisms that included four Gram-positive bacteria (*Staphylococcus aureus* NCTC 6571, *Lysteria monocytogenes* NCTC 11994, *Enterococcus faecalis* ATCC 29212 and *Enterococcus faecium* ATCC 6057), one Gram-negative (*Acinetobacter baumannii* ATCC 19606) and two strains of *Candida* (*C. albicans* ATCC 10231 and *C. parapsilosis* ATCC 22019).

The minimal inhibitory concentration (MIC) values corresponding to the lowest concentration that inhibited the growth after 24 h at 37 °C, were determined according to the standard broth microdilution assays recommended by the National Committee for Clinical Laboratory Standards for bacteria and yeasts (M07-A8 and M27-A2, respectively) and Standards of European Committee on Antimicrobial Susceptibility Testing (EDef7.1). The tested compounds were dissolved in deionized water. The highest tested concentration was 500 μM. The inoculums were 10^5 colony-forming units (cfu mL^{-1}) for bacteria and 10^4 cfu mL^{-1} for *C. albicans* and *C. parapsilosis*. The MIC values were determined in duplicates in three independent experiments.

Cytotoxicity testing. Cytotoxicity in terms of the antiproliferative effect was tested by the 3-(4,5-dimethylthiazol-2-yl)-2,5-diphenyltetrazolium bromide (MTT) assay.[73] The assay was carried out using human lung fibroblasts (MRC5), human cervix cancer (HeLa) and lung cancer (A549) cell lines after 48 h of cell incubation in the medium, containing compounds at concentrations ranging from 0.1 to 400 μM. Briefly, cells were maintained in RPMI-1640 medium supplemented with 100 μg mL^{-1} streptomycin, 100 U mL^{-1} penicillin and 10% (v/v) fetal bovine serum (FBS) (all from Sigma, Munich, Germany) as a monolayer (1×10^4 cells per well) and grown in humidified atmosphere of 95% air and 5% CO_2 at 37 °C. The extent of MTT reduction was measured spectrophotometrically at 540 nm using a Tecan Infinite 200 Pro multiplate reader (Tecan Group Ltd., Männedorf, Switzerland), and the cell survival was expressed as percentage of the control (untreated cells). Cytotoxicity was expressed as the concentration of the compound inhibiting growth by 50% (IC_{50}).

Embryotoxicity and antiangiogenic potential evaluation. Assessment of toxicity and antiangiogenic activity of gold(III) complexes on zebrafish embryos model was carried out according to general rules of the OECD Guidelines for the Testing of Chemicals.[74] All experiments involving zebrafish were performed in compliance with the European directive 86/609/EEC and the ethical guidelines of the Guide for Care and Use of Laboratory Animals of the Institute of Molecular Genetics and Genetic Engineering, University of Belgrade.

Adult zebrafish (*Danio rerio*, wild type) were obtained from a commercial supplier (Pet Center, Belgrade, Serbia), housed in a light- and temperature-controlled facility with 28 °C and standard 14:10-hour light-dark photoperiod, and regularly fed twice a day with commercially dry flake food (TetraMin™ flakes; Tetra Melle, Germany) supplemented with *Artemia nauplii*. Embryos were obtained by natural spawning and raised in the embryo water (0.2 g L^{-1} of Instant Ocean® Salt in distilled water). To examine dose-dependent toxicity of gold(III) complexes, auranofin and the corresponding ligands embryos at 4 - 6 hours post fertilization (hpf) stage were arrayed in 24-well plates, 10 embryos per well, and incubated with 1 mL of embryos water per a well containing various concentrations of the tested compounds at 28 °C. Embryos were exposed to five concentrations of gold(III) complexes **2a**, **2b**, **4a** and **4b**, $K[AuCl_4]$, L-Ala-L-His and L-Leu-L-His (12.5, 25, 50, 75 and 100 μM), and of auranofin (1.25, 2.5, 5, 7.5 and 10 μM). Embryo water alone was used as negative control. Experiments were performed three times using 20 embryos per concentration.

Apical endpoints for toxicity evaluation (Table S6) were recorded at 24, 48, 72, 96 and 114 hpf using an inverted microscope (CKX41; Olympus, Tokyo, Japan). At 114 hpf embryos were inspected for viability, anesthetized by addition of 0.1% (w/v) tricaine solution (Sigma-Aldrich, St. Louis, MO), photographed and killed by freezing at -20 °C for ≥ 24 h.

Transgenic zebrafish embryos *Tg*(*fli1*:*EGFP*) expressing enhanced green fluorescent protein (EGFP) in endothelial cells were kindly obtained from Dr. Ana Cvejic (Wellcome Trust Sanger Institute, Cambridge, UK) and raised in our zebrafish facility to adult stage under previously described life conditions. Transgenic embryos used for the assessment of antiangiogenic potential of the tested compounds were generated by natural spawning of wild type and *Tg*(*fli1*:*EGFP*) adults and reared in embryo water at 28 °C. Embryos staged at 24 hpf were dechorionated with fine tweezers immediately prior to drug treatment, arrayed in 24-well plate with 10 embryos per well, and incubated with 1 mL of embryo water per well containing various concentration of drugs (12.5, 25 and 35 μM) at 28 °C. After drug treatments, zebrafish embryos were anesthetized with 0.003% tricaine (Sigma-Aldrich) and subsequently photographed. The intersegmental blood vessels (ISVs) and subintestinal vessel plexus (SIVs) development were inspected and imaged in embryos at 48 and 72 hpf, respectively under a fluorescence microscope (Olympus BX51,

View Article Online
DOI: 10.1039/C6DT04862E

Applied Imaging Corp., San Jose, CA, USA). Auranofin (Sigma-Aldrich) and sunitinib malate (Suten, Pfizer, New York) were used as a positive controls with known antiangiogenic activity, including in zebrafish embryo model.[30,75]

Molecular docking study

The geometry optimization of studied complexes have been carried out with the application of semi-empirical quantum chemistry method (PM6),[76,77] because of its excellent compromise between computational time and description of electronic correlation.[78] The calculations were performed with the Gaussian 09 molecular package.[79] The crystal structures of human and *E. coli* thioredoxin reductases were obtained from the Brookhaven Protein Data Bank http://www.rcsb.org/pdb (PDB entries: 2ZZ0 and 1TDE, respectively). Molegro Virtual Docker (MVD v. 2013.6.0.1.) software was employed for docking complexes into the rigid enzyme model, for identification of hydrogen bonds and hydrophobic interactions between residues at the active site and for calculation of relevant binding energies.[80] The binding site was computed with a grid resolution of 0.3 Å. The MolDock SE was used as a search algorithm, with the number of runs set to 100. Docking procedure's parameters were: population size 50, maximum number of iterations 1500, energy threshold 100.00 and maximum number of steps 300. The maximum number of generated poses was 10. The estimation of interactions between gold(III) complexes and auranofin, and receptor was described by the MVD-related scoring functions: HBond, NoHBond, steric, VdW, energy, MolDock score, Rerank score, LE1 and LE3. The complex was docked into this grid using the MolDock Optimizer algorithm and its interactions were monitored using detailed energy estimates. A maximum population of 100 and maximum iterations of 10 000 were used for each run and the 5 best poses were retained. For creating two dimensional representations of interactions between complex and enzyme LigPlot+ software was used.[81]

Acknowledgements

This research was financially supported by the Ministry of Education, Science and Technological Development of Serbia (Grant No. 172036 and 173048) and the SupraMedChem@Balkans.Net SCOPES Institutional Partnership (Project No. IZ74Z0_160515). Dr. Ana Cvejic (Wellcome Trust Sanger Institute, Cambridge, UK) is greatly acknowledged for providing transgenic zebrafish embryos and Dr. Željko Vitnik (Department of Chemistry, IChTM Institute of Chemistry, Technology and Metallurgy, University of Belgrade, Belgrade, Serbia) is greatly acknowledged for providing the G09 and computing facilities.

Notes and references

1 I. Sóvágó, K. Várnagy, N. Lihi and Á. Grenács, *Coord. Chem. Rev.*, 2016, **327-328**, 43-54.
2 Y. Qiao, B. Chen, Y. Yang, X. Wang, Y. Xu and H. Li, *Dalton Trans.*, 2016, **45**, 1310-1314.
3 S. Timári, C. Kállay, K. Ősz, I. Sóvágó and K. Várnagy, *Dalton Trans*., 2009, 1962-1971.
4 M. F. Perutz, *Nature*, 1970, **228**, 726-734.
5 J. A. Tainer, E. D. Getzoff, K. M. Beem, J. S. Richardson and D. C. Richardson, *J. Mol. Biol.*, 1982, **160**, 181-217.
6 A. Messerschmidt, A. Rossi, R. Ladenstein, R. Huber, M. Bolognesi, G. Gatti, A. Marchesini, R. Petruzzelli and A. Finazzi-Agró, *J. Mol. Biol*., 1989, **206**, 513-529.
7 V. Lillo and J. R. Galán-Mascarós, *Dalton Trans*., 2014, **43**, 9821-9833.
8 D. Shi, T. W. Hambley and H. C. Freeman, *J. Inorg. Biochem.*, 1999, **73**, 173-186.
9 S. L. Best, T. K. Chattopadhyay, M. I. Djuran, R. A. Palmer, P. J. Sadler, I. Sóvágó and K. Varnagy, *J. Chem. Soc., Dalton Trans.*, 1997, 2587-2596.
10 M. Wienken, E. Zangrando, L. Randaccio, S. Menzer and B. Lippert, *J. Chem. Soc., Dalton Trans*., 1993, 3349-3357.
11 S. U. Milinković, T. N. Parac, M. I. Djuran and N. M. Kostić, *J. Chem. Soc., Dalton Trans.*, 1997, 2771-2776.
12 K. Krogh-Jespersen, J. D. Westbrook, J. A. Potenza and H. J. Schugar, *J. Am. Chem. Soc.*, 1987, **109**, 7025-7031.
13 C. Carbonell, K. C. Stylianou, J. Hernando, E. Evangelio, S. A. Barnett, S. Nettikadan, I. Imaz and D. Maspoch, *Nat. Commun.*, 2013, **4**, 2173.
14 L. Hannibal, S. D. Bunge, R. van Eldik, D. W. Jacobsen, C. Kratky, K. Gruber and N. E. Brasch, *Inorg. Chem.*, 2007, **46**, 3613-3618.
15 H. Yue, D. Zhang, Y. Chen, Z. Shi and S. Feng, *Inorg. Chem. Commun.*, 2006, **9**, 959-961.
16 L. Wang, J. Cai, Z.-W. Mao, X.-L. Feng and J.-W. Huang, *Transition Met. Chem.*, 2004, **29**, 411-418.
17 H. Preut, M. Vornefeld and F. Huber, *Acta Crystallogr., Sect. C: Cryst. Struct. Commun*., 1991, **47**, 264-267.
18 R. Dreos, L. Mechi, G. Nardin, L. Randaccio and P. Siega, *J. Organomet. Chem.*, 2005, **690**, 3815-3821.
19 M. Wienken, B. Lippert, E. Zangrando and L. Randaccio, *Inorg. Chem*., 1992, **31**, 1983-1985.
20 U. Rychlewska, B. Warżajtis, B. Đ. Glišić, M. D. Živković, S. Rajković and M. I. Djuran, *Dalton Trans*., 2010, **39**, 8906-8913.
21 B. Đ. Glišić, S. Rajković and M. I. Djuran, *J. Coord. Chem.*, 2013, **66**, 424-434.
22 B. Đ. Glišić, U. Rychlewska and M. I. Djuran, *Dalton Trans*., 2012, **41**, 6887-6901.
23 B. Đ. Glišić, S. Rajković, M. D. Živković and M. I. Djuran, *Bioorg. Chem*., 2010, **38**, 144-148.
24 S. Carotti, G. Marcon, M. Marussich, T. Mazzei, L. Messori, E. Mini and P. Orioli, *Chem. Biol. Interact.,* 2000, **125**, 29-38.
25 I. Ott, *Coord. Chem. Rev.,* 2009, **253**, 1670-1681.
26 N. J. Farrer and P. J. Sadler, Medicinal inorganic chemistry: state of the art, new trends, and a vision of the future, in *Bioinorganic Medicinal Chemistry*, ed. E. Alessio, Wiley-VCH Verlag GmbH & Co. KGaA, Wienheim, 2011, pp. 1-48.
27 S.-H. Park, J. H. Lee, J. S. Berek and M. C.-T. Hu, *Int. J. Oncol*., 2014, **45**, 1691-1698.
28 M. I. Cassetta, T. Marzo, S. Fallani, A. Novelli and L. Messori, *Biometals*, 2014, **27**, 787-791.
29 M. B. Harbut, C. Vilchèze, X. Luo, M. E. Hensler, H. Guo, B. Yang, A. K. Chatterjee, V. Nizet, W. R. Jacobs, P. G. Schultz and F. Wang, *Proc. Natl. Acad. Sci. U.S.A.*, 2015, **112**, 4453-4458.
30 M.-F. He, X.-P. Gao, S.-C. Li, Z.-H. He, N. Chen, Y.-B. Wang and J.-X. She, *Eur. J. Pharmacol.,* 2014, **740**, 240-247.
31 R. Křikavová, J. Hošek, P. Suchý, Jr., J. Vančo and Z. Trávníček, *J. Inorg. Biochem.,* 2014, **134**, 92-99.

DOI: 10.1039/C6DT04862E

32 B. Đ. Glišić, S. Rajković, Z. D. Stanić and M. I. Djuran, *Gold Bull*., 2011, **44**, 91-98.
33 U. Rychlewska, B. Warżajtis, B. Đ. Glišić, S. Rajković, M. I. Djuran, *Acta Crystallogr., Sect. C: Cryst. Struct. Commun*., 2010, **66**, 51-54.
34 T. G. Appleton, F. J. Pesch, M. Wienken, S. Menzer and B. Lippert, *Inorg. Chem*., 1992, **31**, 4410-4419.
35 Ts. Kolev, B. B. Koleva, S. Y. Zareva and M. Spiteller, *Inorg. Chim. Acta*, 2006, **359**, 4367-4376.
36 N. S. Drašković, D. D. Radanović, U. Rychlewska, B. Warżajtis, I. M. Stanojević and M. I. Djuran, *Polyhedron*, 2012, **43**, 185-193.
37 N. Pantelić, T. P. Stanojković, B. B. Zmejkovski, T. J. Sabo and G. N. Kaluđerović, *Eur. J. Med. Chem*., 2015, **90**, 766-774.
38 A. Bondi, *J. Phys. Chem.,* 1964, **68**, 441-451.
39 B. Đ. Glišić and M. I. Djuran, *Dalton Trans.*, 2014, **43**, 5950-5969
40 N. S. Radulović, N. M. Stojanović, B. Đ. Glišić, P. J. Randjelović, Z. Z. Stojanović-Radić, K. V. Mitić, M. I. Djuran, *unpublished results*
41 D. Trofa, A. Gácser and J. D. Nosanchuk, *Clin. Microbiol, Rev.*, 2008, **21**, 606-625.
42 M. B. Dinger and W. Henderson, *J. Organomet. Chem*., 1998, **560**, 233-243.
43 K. J. Kilpin, W. Henderson and B. K. Nicholson, *Polyhedron*, 2007, **26**, 204-213.
44 K. J. Kilpin, W. Henderson and B. K. Nicholson, *Polyhedron*, 2007, **26**, 434-447.
45 N. D. Savić, D. R. Milivojevic, B. Đ. Glišić, T. Ilic-Tomic, J. Veselinovic, A. Pavic, B. Vasiljevic, J. Nikodinovic-Runic and M. I. Djuran, *RSC Adv.*, 2016, **6**,13193–13206.
46 B. Đ. Glišić, N. D. Savić, B. Warżajtis, L. S. Djokic, T. Ilic-Tomic, M. Antić, S. Radenković, J. Nikodinovic-Runic, U. Rychlewska, M. I. Djuran, *MedChemComm*, 2016, **7**, 1356-1366.
47 R. V. Parish, B. P. Howe, J. P. Wright, J. Mack, R. G. Pritchard, R. G. Buckley, A. M. Elsome and S. P. Fricker, *Inorg. Chem*., 1996, **35**, 1659-1666.
48 R. V. Parish, J. Mack, L. Hargreaves, J. P. Wright, R. G. Buckley, A. M. Elsome, S. P. Fricker and B. R. C. Theobald, *J. Chem. Soc., Dalton Trans*., 1996, 69-74.
49 T. Zou, C. T. Lum, C.-N. Lok, J.-J. Zhang and C.-M. Che, *Chem. Soc. Rev.*, 2015, **44**, 8786-8801.
50 L. Messori, F. Abbate, G. Marcon, P. Orioli, M. Fontani, E. Mini, T. Mazzei, S. Carotti, T. O'Connell and P. Zanello, *J. Med. Chem.*, 2000, **43**, 3541-3548.
51 S. Nobili, E. Mini, I. Landini, C. Gabbiani, A. Casini and L. Messori, *Med. Res. Rev.,* 2010, **30**, 550-580.
52 A. Casini, G. Kelter, C. Gabbiani, M. A. Cinellu, G. Minghetti, D. Fregona, H.-H. Fiebig and L. Messori, *J. Biol. Inorg. Chem.,* 2009, **14**, 1139-1149.
53 V. Gandin, A. P. Fernandes, M. P. Rigobello, B. Dani, F. Sorrentino, F. Tisato, M. Björnstedt, A. Bindoli, A. Sturaro, R. Rella and C. Marzano, *Biochem. Pharmacol.*, 2010, **79**, 90-101.
54 L. Messori, G. Marcon, M. A. Cinellu, M. Coronnello, E. Mini, C. Gabbiani and P. Orioli, *Bioorg. Med. Chem*., 2004, **12**, 6039-6043.
55 L. Ronconi, L. Giovagnini, C. Marzano, F. Bettìo, R. Graziani, G. Pilloni and D. Fregona, *Inorg. Chem*., 2005, **44**, 1867-1881.
56 C. A. MacRae and R. T. Peterson, *Nat. Rev. Drug Discov*., 2015, **14**, 721-731.
57 T. A. C. Newman, C. R. Carleton, B. Leeke, M. B. Hampton and J. A. Horsfield, *Redox Biol*., 2015, **6**, 648-655.
58 X.-Y. Gao, K. Li, L.-L. Jiang, M.-F. He, C.-H. Pu, D. Kang and J. Xie, *J. Appl. Toxicol.*, 2016, DOI: 10.1002/jat.3410.
59 S. Lin, Y. Zhao, Z. Ji, J. Ear, C. H. Chang, H. Zhang, C. Low-Kam, K. Yamada, H. Meng, X. Wang, R. Liu, S. Pokhrel, L. Mädler L, R. Damoiseaux, T. Xia, H. A. Godwin, S. Lin and A. E. Nel, *Small*, 2013, **9**, 1776-1785.
60 N. D. Savić, S. Vojnovic, B. Đ. Glišić, M. Antić, S. Radenković, B. Warżajtis, U. Rychlewska, J. Nikodinovic-Runic, M. I. Djuran and A. Pavic, *submitted*
61 J. Folkman, *Nat. Med.*, 1995, **1**, 27-30.
62 P. Carmeliet and R. K. Jain, *Nature*, 2000, **407**, 249-257.
63 L. L. Dunn, A. M. Buckle, J. P. Cooke and M. K. C. Ng, *Arterioscler. Thromb. Vasc. Biol.*, 2010, **30**, 2089-2098.
64 C. Tobia, G. Gariano, G. De Sena and M. Presta, *Biochim. Biophys. Acta*, 2013, **1832**, 1371-1377.
65 C. Marzano, V. Gandin, A. Folda, G. Scutari, A. Bindoli and M. P. Rigobello, *Free Radic. Biol. Med.,* 2007, **42**, Pages 872-881.
66 R. T. Kroemer, *Curr. Protein Pept. Sci*., 2007, **8**, 312-328.
67 A. Kreźel and W. Bal, *J. Inorg. Biochem*., 2004, **98**, 161-166.
68 *CrysAlis PRO*, Agilent Technologies, Yarnton, Oxfordshire, England, 2014.
69 R. C. Clark and J. S. Reid, *Acta Crystallogr., Sect. A: Found. Crystallogr*., 1995, **51**, 887-897.
70 G. M. Sheldrick, *Acta Crystallogr., Sect. A: Found. Crystallogr*., 2008, **64**, 112-122.
71 H. D. Flack, *Acta Crystallogr., Sect. A: Found. Crystallogr*., 1983, **39**, 876–881.
72 I. J. Bruno, J. C. Cole, P. R. Edgington, M. Kessler, C. F. Macrae, P. McCabe, J. Pearson and R. Taylor, *Acta Crystallogr., Sect. B: Struct. Sci*., 2002, **58**, 389-397.
73 M. B. Hansen, S. E. Nielsen and K. Berg, *J. Immunol. Methods*, 1989, **119**, 203-210.
74 OECD, OECD Guidelines for the Testing of Chemicals, 2013 Test no. 236.
75 G. Chimote, J. Sreenivasan, N. Pawar, J. Subramanian, H. Sivaramakrishnan and S. Sharma, *Drug Des. Devel. Ther.*, 2014, **8**, 1107-1123.
76 E. A. Amin and D. G. Truhlar, *J. Chem. Theory Comput*., 2008, **4**, 75-85.
77 J. J. P. Stewart, *J. Mol. Model*., 2007, **13**, 1173-1213.
78 G. Frison and G. Ohanessian, *J. Comput. Chem*., 2008, **29**, 416-433.
79 M. J. Frisch, et al., Gaussian 09, Revision C.02, Wallingford, CT, 2004.
80 R. Thomsen and M. H. Christensen, *J. Med. Chem*., 2006, **49**, 3315-3321.
81 R. A. Laskowski and M. B. Swindells, *J. Chem. Inf. Model*., 2011, **51**, 2778-2786.

View Article Online
DOI: 10.1039/C6DT04862E

Graphical abstract

Mononuclear gold(III) complexes with L-histidine-containing dipeptides: tuning the structural and biological properties by variation of the N-terminal amino acid and counter anion

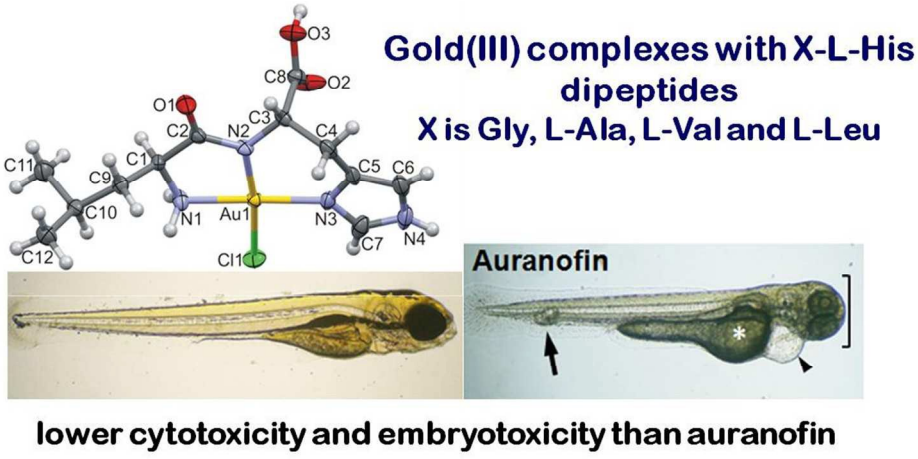

Cytotoxicity and embryotoxicity of gold(III) complexes with L-histidine-containing dipeptides, in which N-terminal amino acid is L-alanine and L-leucine, were significantly lower in comparison to auranofin, making them good candidates for further development towards antiangiogenic drugs.